

Near Infrared Shielding Properties of Quaternary Tungsten Bronze Nanoparticle $\text{Na}_{0.11}\text{Cs}_{0.22}\text{WO}_3$

Kyunghwan Moon,^a Jin-Ju Cho,^a Ye-Bin Lee, Pil J. Yoo,[†] Chung Wung Bark,[‡] and Juhyun Park^{*}

School of Chemical Engineering and Materials Science, Chung-Ang University, Seoul 156-756, Korea

*E-mail: jpark@cau.ac.kr

[†]School of Chemical Engineering and SKKU Advanced Institute of Nanotechnology (SAINT), Sungkyunkwan University, Suwon 440-746, Korea

[‡]Department of Electrical Engineering, Gachon University, Gyunggi-Do 461-701, Korea

Received November 9, 2012, Accepted December 4, 2012

Reduced tungsten bronze nanoparticles of ternary and quaternary compounds were prepared by adding sodium and cesium to crystal structures of tungsten trioxides ($\text{Na}_x\text{Cs}_{0.33-x}\text{WO}_3$, $x = 0, 0.11$) while maintaining the overall alkali metal fraction at 0.33, in an attempt to control near infrared (NIR) shielding property in the particular wavelength range of 780 to 1200 nm. The structure and composition analysis of the quaternary compound, $\text{Na}_{0.11}\text{Cs}_{0.22}\text{WO}_3$, revealed that 93.1% of the hexagonal phase was formed, suggesting that both alkali metals were mainly inserted in hexagonal channel. The NIR shielding property for $\text{Na}_{0.11}\text{Cs}_{0.22}\text{WO}_3$ was remarkable, as this material demonstrated efficient transmittance of visible light up to 780 nm and enhancement in NIR shielding because of the blue-shifted absorption maximum in comparison to $\text{Cs}_{0.33}\text{WO}_3$.

Key Words : Tungsten bronze, Near infrared, Energy saving windows, Solar filter

Introduction

The shielding of near infrared (NIR, wavelength of 780 to 2500 nm) radiation has been a global issue in recent years as societies seek to reduce energy consumption for environmental preservation.¹ Thin film coatings on the windows of automobiles and buildings are used to filter out heat waves while retaining high transparency for visible light, thus significantly increasing air conditioning efficiency in summer and heating efficiency in winter. A variety of thin film coating materials and technologies have been studied in academia and industry including rare-earth hexaborides,² indium tin oxides,^{3,4} antimony-doped tin oxides,⁵ and Low-E glasses.⁶ However, ideal NIR absorbents are still in high demand due to the limitations of current technologies, such as low visible light transparency,² partial NIR shielding,^{3,4} and high cost of material or processing.⁶

Tungsten bronze nanoparticles, consisting of tungsten trioxides with alkali metal additives, are one of the most promising candidates for NIR shielding applications. When alkali metals are incorporated into crystal structures of tungsten trioxides (WO_3), it is accepted that electrons are donated by the alkali atoms to the conduction band of WO_3 , forming surface plasmon polariton of free electrons and introducing empty, higher sub-bands or states in the conduction band.⁷⁻⁹ Thus, upon light irradiation, electrons are activated from occupied states in the conduction band to empty states. The energy for this activation is matched with the NIR wavelength, thus providing NIR shielding effect for substrates coated with tungsten bronze thin films. Adachi

et al. investigated the optical properties of tungsten bronze nanoparticles (M_xWO_3 , $\text{M} = \text{Na}, \text{Tl}, \text{Rb}, \text{and Cs}$) that were prepared using a solid state reaction and milling.¹⁰ It was revealed that cesium tungsten bronzes with a hexagonal crystal structure ($\text{Cs}_{0.33}\text{WO}_3$) are highly suitable for solar filters, in which the metal fraction is limited to 0.33 at maximum to maintain the hexagonal phase. Guo *et al.* and Yin *et al.* further demonstrated the excellence of the cesium tungsten bronzes as NIR absorbents by synthesizing Cs_xWO_3 nanorods *via* a water controlled-release solvothermal process.¹¹⁻¹³

In this paper, tungsten bronze nanoparticles with a quaternary element ($\text{Na}_x\text{Cs}_{0.33-x}\text{WO}_3$, $x = 0.11$) were prepared using a traditional solid state reaction and a mechanical ball-mill process in an attempt to control NIR shielding property in the wavelength range of 780 to 1200 nm. Current research has focused primarily on ternary compounds of tungsten bronzes, with sodium or cesium tungsten bronze (Na_xWO_3 or Cs_xWO_3) displaying the most remarkable NIR shielding properties. However, an attempt to improve NIR shielding is still necessary, as current technologies are insufficient, cutting off only approximately 60% of heat rays near 780 nm, although nearly perfect NIR shielding above 1200 nm has been achieved. We introduced the fourth element of sodium into the cesium tungsten bronze compound while maintaining the overall alkali metal fraction at 0.33. Since sodium tungsten bronzes has the absorption maximum with a shorter wavelength and a narrower band width than those of cesium tungsten oxides because of more localized electronic states, it is expected that in comparison to $\text{Cs}_{0.33}\text{WO}_3$, the resulting quaternary tungsten bronze nanoparticles will show an improved NIR shielding property specifically in the range of

^aThese authors contributed equally to this work.

780 to 1200 nm due to modulated optical response by the quaternary element of sodium.

Experimentals

Ammonium tungsten oxide hydrate ($(\text{NH}_4)_6\text{W}_{12}\text{O}_{39}\cdot x\text{H}_2\text{O}$, Alfa Aesar), cesium carbonate (Cs_2CO_3 , Sigma-Aldrich Co.) and sodium carbonate (Na_2CO_3 , Samchun Chemical Co.) were dissolved in deionized water at predetermined molar ratios of Na/Cs/W (0.11/0.22/1, 0/0.33/1) and dried overnight in a vacuum at 80 °C. The resulting powders were placed in a crucible inside a thermal CVD furnace and reacted using a three-step procedure. The furnace atmosphere was replaced with an argon gas flow prior to heating, and with a gas mixture flow ($\text{H}_2:\text{Ar} = 95:5$) after the furnace temperature reached 350 °C. The powders were then heated at 550 °C for 1 h and annealed at 800 °C in an argon atmosphere for 1 h. The resulting microcrystals of tungsten bronzes, exhibiting a deep blue color, were mixed with toluene and BYK-182 dispersant (Disperbyk-182, BYK Chemie) at a ratio of microcrystal/toluene/BYK-182 = 8/84/8 (w/w/w), and were vigorously shaken with 0.5 mm zirconia beads in a ball miller (MTI, High Speed Vibration Ball Miller) for 8 h to produce nanoparticles.

The crystal structures of tungsten bronze nanoparticles were characterized using an X-ray diffractometer (XRD, Bruker-AXS NEW D8-Advance) and a field emission scanning electron microscope (FE-SEM, SIGMA, Carl Zeiss). Nanoparticle sizes were measured with a particle analyzer (PSA, OTSUKA ELS-Z) and a field emission transmission electron microscope (FE-TEM, FEI Tecnai G2 F30 S-Twin). The compositions were determined using an energy dispersive spectrometer (EDS, Thermo Scientific NORAN System 7) and X-ray photoelectron spectroscopy (XPS, $h\nu = 1486.6$ eV Al $K\alpha$). Absorption and transmission spectra were obtained using a spectrophotometer (JASCO V-670) in a range of 300 to 2100 nm.

Results and Discussion

The tungsten bronzes as prepared above formed microcrystals that ranged in size from 0.1–1 μm , as representative-

ly shown in the SEM image of $\text{Na}_{0.11}\text{Cs}_{0.22}\text{WO}_3$ microcrystals in Figure 1(a). Because the free carrier density and visible light transparency increase with decreasing the crystal size and increasing surface free electrons,⁷ the microcrystals mentioned above (Figure 1(a)) were collided to nanoparticles in a conventional ball milling process to maximize the activation of free electrons in the tungsten bronzes. The resulting tungsten bronze nanoparticles are ranged in size from 80 to 120 nm averaged at 106 nm, as confirmed by the TEM image and particle analysis data illustrated in Figure 1(b) and 1(c) for $\text{Na}_{0.11}\text{Cs}_{0.22}\text{WO}_3$ nanoparticles.

The compositions of tungsten bronze nanoparticles were determined using XPS spectra of the core-level tungsten (W_{4f}) and EDS analysis. The XPS spectra shown in Figure 2(a) and (b) were fitted as two spin-orbit doublets, $\text{W}_{4f_{5/2}}$ and $\text{W}_{4f_{7/2}}$, with an interval of 2.34 eV. The peaks at 33.79–33.99 ($\text{Cs}_{0.33}\text{WO}_3$, Figure 2(a)) and 35.47–35.67 eV ($\text{Na}_{0.11}\text{Cs}_{0.22}\text{WO}_3$, Figure 2(b)) were attributed to W^{5+} , and those at 36.13–36.33 ($\text{Cs}_{0.33}\text{WO}_3$, Figure 2(a)), and 37.81–38.01 eV ($\text{Na}_{0.11}\text{Cs}_{0.22}\text{WO}_3$, Figure 2(b)) to W^{6+} , respectively.¹⁴ Upon adding alkali metals to WO_3 , accompanied by electron donation, W^{6+} is reduced to W^{5+} . The compositions of $\text{Na}_x\text{Cs}_{0.33-x}\text{WO}_3$ could thus be estimated using an area analysis of the doublet peaks. The metal fraction x in $\text{Na}_x\text{Cs}_{0.33-x}\text{WO}_3$ was determined and is summarized in Table 1. This is coincident with the molar ratio of reactant mixtures. EDS and XPS analysis produced the same compositions for all samples and a representative EDS spectrum for $\text{Na}_{0.11}\text{Cs}_{0.22}\text{WO}_3$ nanoparticles is shown in Figure 2(c).

The crystal structures of tungsten bronze nanoparticles were analyzed using the XRD patterns and summarized in Figure 3. For the ternary compounds, XRD peaks for $\text{Cs}_{0.33}\text{WO}_3$ nanoparticles were clearly indexed to the cesium hexagonal tungsten bronze phase (Cs-HTB, $\text{Cs}_{0.30}\text{WO}_3$, PDF 01-083-1334) (Figure 3(a)). The quaternary compound of $\text{Na}_{0.11}\text{Cs}_{0.22}\text{WO}_3$ presents hexagonal crystal structures as shown in Figure 3(c); however, a detailed analysis reveals that a small portion of the cubic phase is mixed with the hexagonal phase. When the XRD pattern of the quaternary compounds was decomposed by using the Pawley and Le Bail method, 93.1% of the hexagonal phase ($\text{Cs}_{0.32}\text{WO}_3$, PDF 01-083-1334, space group = $\text{P}63/\text{mcm}$, $a = 7.41$ Å, $c =$

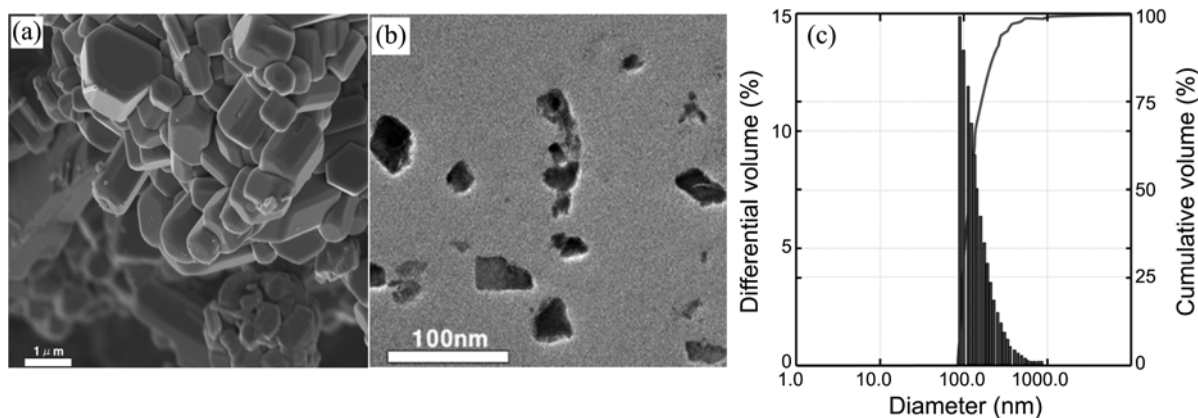


Figure 1. (a) SEM image of $\text{Na}_{0.11}\text{Cs}_{0.22}\text{WO}_3$ microcrystals; (b) TEM image and (c) particle size distributions of $\text{Na}_{0.11}\text{Cs}_{0.22}\text{WO}_3$ nanoparticles.

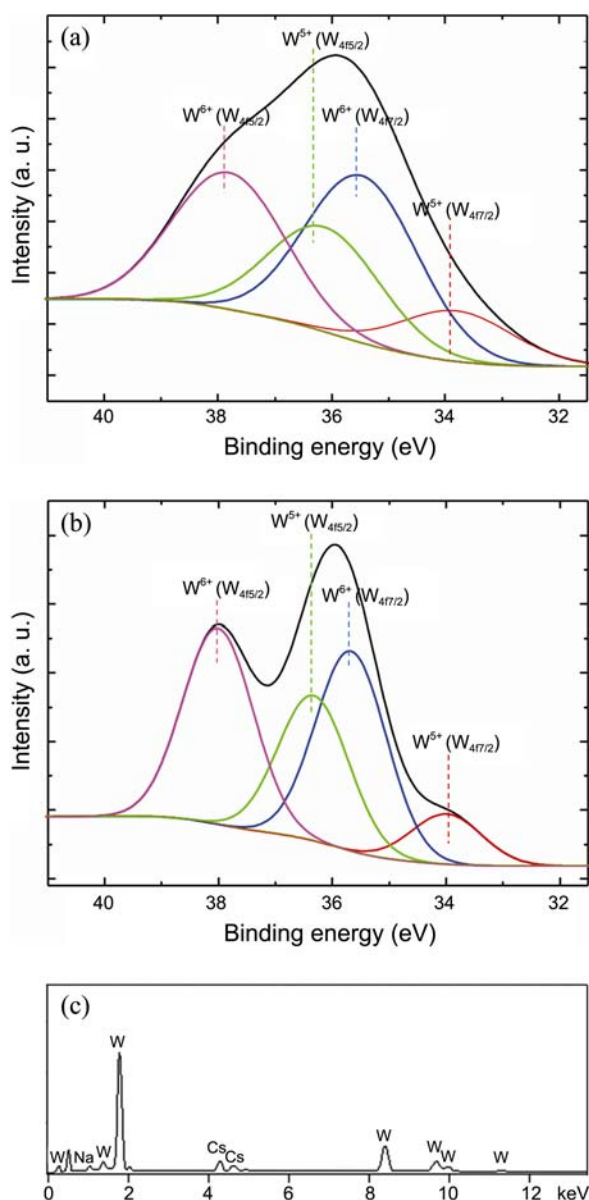


Figure 2. W_{4f} core-level XPS spectra of (a) $Cs_{0.33}WO_3$, (b) $Na_{0.11}Cs_{0.22}WO_3$ nanoparticles and (c) EDS analysis of $Na_{0.11}Cs_{0.22}WO_3$ nanoparticles.

7.60 Å) and 6.93% of the cubic phase ($Na_{0.11}WO_3$, PDF 01-075-0057, space group = Pm-3m, $a = 3.84$ Å) were found for $Na_{0.11}Cs_{0.22}WO_3$. It appears that with our solid state reaction conditions for the quaternary tungsten bronze and at the metal fraction of $x = 0.11$, the formation of the cubic phase is drastically reduced. The cubic phase is generally formed for a ternary compound of sodium tungsten bronze (Na_xWO_3) where x is in range of 0.3 to 1.0 relative to tungsten.^{15,16} Also, for the ternary compound of $Na_{0.11}WO_3$, the tetragonal crystal structure is typically found.¹⁵ In our result, the cubic phase was formed at the sodium fraction of 0.11 possibly due to our high temperature solid state reaction condition for a quaternary compound. The portion of the cubic phase can be up to 33% as the addition ratio of sodium and cesium is 1:2 in the quaternary compound. The structure analysis data

Table 1. Binding energies of two spin-orbit doublets, $W_{4f_{5/2}}$ and $W_{4f_{7/2}}$, for the interval of 2.34 eV, as attributed to W^{5+} and W^{6+} in $Na_xCs_{0.33-x}WO_3$ nanoparticles, and the estimated metal fraction x

Sample	W^{5+}		W^{6+}		Sodium fraction x
	$W_{4f_{5/2}}$ (eV)	$W_{4f_{7/2}}$ (eV)	$W_{4f_{5/2}}$ (eV)	$W_{4f_{7/2}}$ (eV)	
$Cs_{0.33}WO_3$	33.79	35.47	36.13	37.81	0
$Na_{0.11}Cs_{0.22}WO_3$	33.99	35.67	36.33	38.01	0.11

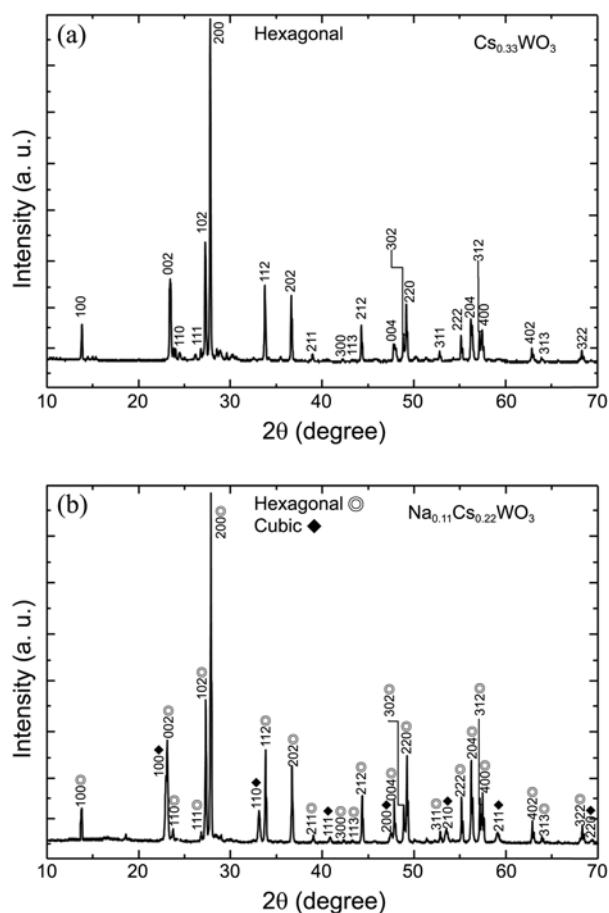


Figure 3. XRD patterns of $Na_xCs_{0.33-x}WO_3$ nanoparticles where (a) $x = 0$ and (b) $x = 0.11$.

which reveal 93.1% of the hexagonal phase and the composition analysis data which show the 0.11:0.22 addition ratio of sodium and cesium in the quaternary compound indicate that both alkali metals are primarily incorporated into the hexagonal channels of WO_3 . Thus it seems that the larger alkali metal element of cesium drives the formation of the hexagonal phase and that sodium can easily be intercalated into the hexagonal channel due to its small size. The easier diffusion of small elements such as hydrogen and lithium through the hexagonal framework of cesium tungsten bronzes was reported elsewhere.¹⁷ As a result, only 6.9% of the cubic phase is formed in $Na_{0.11}Cs_{0.22}WO_3$.

Figure 4(a) shows various nanoparticle absorption spectra. Cesium tungsten bronze nanoparticles of $Cs_{0.33}WO_3$ showed a broader absorption above 900 nm, with a maximum at λ_{max}

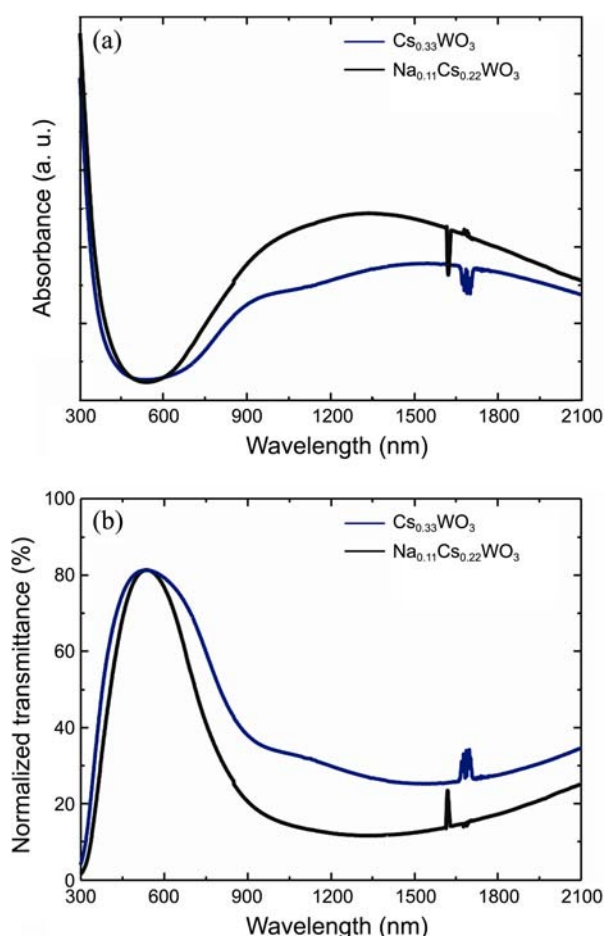


Figure 4. (a) Absorption and (b) transmittance spectra of $\text{Na}_x\text{Cs}_{0.33-x}\text{WO}_3$ nanoparticles dispersed at 0.01 wt % in toluene, where $x = 0$ and 0.11. The spectra between 1620 and 1790 nm were disturbed by toluene. The transmittance spectra were normalized at 80% transmittance in the visible region to clearly demonstrate the shift of the NIR shielding region, depending on metal compositions.

= 1600 nm, which matches well the result from the currently published literature.⁵ These features indicate that the band structures of $\text{Cs}_{0.33}\text{WO}_3$, formed by electron contribution from metal ions to the tungsten conduction band, are delocalized possibly due to the incorporation of large cesium element, resulting in more distorted crystal structures.¹⁵ Cs-HTBs can thus show good performance for NIR shielding in a wider range of NIR wavelength. When sodium is added to the Cs-HTBs at a 0.11 mole fraction while maintaining the overall metal fraction at 0.33, the resulting $\text{Na}_{0.11}\text{Cs}_{0.22}\text{WO}_3$ nanoparticles present a broad absorption similar to Cs-HTBs. However, the absorption maximum is blue-shifted to 1325 nm, reflecting the sodium addition effect and enhancing absorption in the range of 780 to 1200 nm. These results suggest that the cesium addition to the tungsten trioxide contributes to the broader band absorption due to the delocalized electronic states by the larger element and that the smaller sodium element can modify the optical property of the resulting quaternary tungsten bronze due to less the delocalized electronic states and shorter absorption band of sodium tungsten bronze while preserving the hexagonal

framework.

The transmittance spectra of $\text{Na}_x\text{Cs}_{0.33-x}\text{WO}_3$ nanoparticles in Figure 4(b) clearly reflect the absorption properties illustrated in Figure 4(a). The maximum visible light transmission for $\text{Cs}_{0.33}\text{WO}_3$ and $\text{Na}_{0.11}\text{Cs}_{0.22}\text{WO}_3$ occurred at wavelengths of 531 and 538 nm respectively. Approximately 60 to 80% of the NIR were cut off in the range of 900 to 2100 nm. It is important to note that NIR shielding property in the range of 780 to 1200 nm was significantly improved when a 0.11 mole fraction of sodium was inserted into Cs-HTBs.

Conclusion

Tungsten bronze nanoparticles of $\text{Na}_x\text{Cs}_{0.33-x}\text{WO}_3$ were prepared using a solid state reaction procedure, and the effect of varying alkali metal compositions on NIR shielding properties was investigated. The NIR shielding properties showed remarkable enhancement in the range of 780 to 1200 nm in the quaternary compound of $\text{Na}_{0.11}\text{Cs}_{0.22}\text{WO}_3$. These results suggest that the preservation of the hexagonal phase in Cs-HTBs with sodium addition is highly plausible for preparing solar filters, which can effectively shield all wavelengths of NIR. A bottom-up synthesis of well-defined $\text{Na}_x\text{Cs}_{0.33-x}\text{WO}_3$ nanocrystals might provide one of the best NIR absorbers; notwithstanding, controlling metal composition for quaternary compounds in the bottom-up synthesis is still challenging, requiring an area for further research.

Acknowledgments. This research was supported by the Chung-Ang University Research Grants in 2009.

References

- Hamberg, I.; Granqvist, C. G. *J. Appl. Phys.* **1986**, *60*, R123.
- Adachi, K.; Miratsu, M.; Asahi, T. *J. Mater. Res.* **2010**, *25*, 510.
- Okada, M.; Yamada, Y.; Jin, P.; Tazawa, M.; Yoshimura, K. *Thin Solid Films* **2003**, *442*, 217.
- Kanehara, K.; Koike, H.; Yoshinaga, T.; Teranishi, T. *J. Am. Chem. Soc.* **2009**, *131*, 17736.
- Takeda, H.; Adachi, K. *J. Am. Ceram. Soc.* **2007**, *90*, 4059.
- Carmody, J.; Selkowitz, S.; Hescong, L. *Residential Windows: A Guide to New Technologies and Energy Performance*, 1st ed.; W. W. Norton & Company: New York, 1996.
- Green, M.; Travlos, A. *Philos. Mag. B* **1985**, *51*, 501.
- Lynch, D. W.; Rosei, R.; Weaver, J. H.; Olson, C. G. *J. Solid State Chem.* **1973**, *8*, 242.
- Schirmer, O. F.; Wittwer, W.; Baur, G.; Brandt, G. *J. Electrochem. Soc.* **1977**, *124*, 749.
- Takeda, H.; Adachi, K. *J. Am. Ceram. Soc.* **2007**, *90*, 4059.
- Guo, C.; Yin, S.; Zhang, P.; Yan, M.; Adachi, K.; Chonan, T.; Sato, T. *J. Mater. Chem.* **2010**, *20*, 8227.
- Guo, C.; Yin, S.; Huang, L.; Yang, L.; Sato, T. *Chem. Commun.* **2011**, *47*, 8853.
- Guo, C.; Yin, S.; Yan, M.; Sato, T. *J. Mater. Chem.* **2011**, *21*, 5099.
- Liu, J.-X.; Ando, Y.; Dong, X.-L.; Shi, F.; Yin, S.; Adachi, K.; Chonan, T.; Tanaka, A.; Sato, T. *J. Solid State Chem.* **2010**, *183*, 2456.
- Raj, S.; Matsui, H.; Souma, S.; Sato, T.; Takahashi, T.; Chakraborty, A.; Sarma, D. D.; Mahadevan, P.; Oishi, S.; McCarroll, W. H.; Greenblatt, M. *Phys. Rev. B* **2007**, *75*, 155116.
- Hgg, G. *Nature* **1935**, *3421*, 874.
- Zhong, Q.; Colbow, K. *Thin Solid Films* **1991**, *196*, 305.